Ordered Nanoparticles Hot Paper

International Edition: DOI: 10.1002/anie.201603022
German Edition: DOI: 10.1002/ange.201603022

Ordered PdCu-Based Nanoparticles as Bifunctional Oxygen-Reduction and Ethanol-Oxidation Electrocatalysts

Kezhu Jiang[+], Pengtang Wang[+], Shaojun Guo, Xu Zhang, Xuan Shen, Gang Lu, Dong Su, and Xiaoqing Huang**

Abstract: *The development of superior non-platinum electrocatalysts for enhancing the electrocatalytic activity and stability for the oxygen-reduction reaction (ORR) and liquid fuel oxidation reaction is very important for the commercialization of fuel cells, but still a great challenge. Herein, we demonstrate a new colloidal chemistry technique for making structurally ordered PdCu-based nanoparticles (NPs) with composition control from PdCu to PdCuNi and PtCuCo. Under the dual tuning on the composition and intermetallic phase, the ordered PdCuCo NPs exhibit better activity and much enhanced stability for ORR and ethanol-oxidation reaction (EOR) than those of disordered PdCuM NPs, the commercial Pt/C and Pd/C catalysts. The density functional theory (DFT) calculations reveal that the improved ORR activity on the PdCuM NPs stems from the catalytically active hollow sites arising from the ligand effect and the compressive strain on the Pd surface owing to the smaller atomic size of Cu, Co, and Ni.*

Fuel cells are considered as potential power sources for automotives and portable electronic devices as they are highly promising candidates for providing sustainable, clean, and efficient energy supply.[1,2] The development of highly efficient catalysts for anodic and cathodic reactions is crucial for the development of fuel-cell technologies.[3,4] Among all the catalysts studied, Pt and its alloy are of more interest because of their high activity for both the anodic oxidation reaction and the cathodic oxygen-reduction reaction (ORR).[5–9] However, the practical large-scale commercialization of fuel cells is still a formidable challenge because of two key challenging issues related to very low abundance of Pt in nature and poor long-term duration.[10–13] One of interesting strategies is to develop Pd-based nanocatalysts with catalytic performance comparable to or even superior to that of Pt, because of their great potential in catalyzing reduction of oxygen and the electrochemical oxidation of small organic molecules.[14–17] Inspired by this, great efforts have been focused on the rational design of multicomponent Pd-based NPs with desired size, composition, and shape tunings to further improve the performance of Pd-based fuel-cell nanocatalysts.[18,19] However, these previous studies mainly focus on the conventional disordered Pd-based multimetallic nanocatalysts.[20,21] Such disordered structure suffers from low stability in the corrosive electrochemical environment and only moderate activity improvement.[22,23] From the structural perspective, the ordered intermetallic phases, with definite composition and structure, can provide the predictable control over structural, geometric, and electronic effects for catalysis optimization, which cannot be afforded by the widely created conventional alloys.[24–26] Especially, the ordered intermetallic nanocrystals usually exist the strong electron interaction and the change of the bond length and electron configuration, which could significantly improve their catalytic activities for both ORR and oxidation reactions of fuels.[27]

In this regard, if we can engineer multicomponent Pd-based NPs with ordered intermetallic phases, it will be extremely beneficial for the creation of Pd-based catalysts with both enhanced activity and stability. Herein we report our research efforts in developing a general method for the controlled synthesis of multicomponent Pd-based NPs with a structurally ordered intermetallic feature. A series of PdCu-based trimetallic NPs, including PdCu, PdCuNi, and PtCuCo can be produced by a large-scalable wet-chemical approach. These monodisperse PdCuM NPs can be readily converted into structurally ordered intermetallic ones through the simple annealing treatment at 375 °C. The newly generated class of structurally ordered intermetallic PdCuM NPs shows the interesting M composition-dependent electrocatalytic performance with Co being the best ORR and ethanol-oxidation reaction (EOR) activities. Under the dual tuning on the composition and intermetallic phase, the ordered PdCuCo NPs exhibit much better activity and stability towards both the ORR and EOR than the disordered PdCuM NPs. Specifically, the PdCuCo NPs show 1.3 and 3.3 times higher mass activities for ORR, and 12.9 and 17.5 times higher mass activities for EOR than commercial Pt/C and Pd/C catalysts,

[*] K. Jiang,[+] P. Wang,[+] Prof. X. Huang
College of Chemistry
Chemical Engineering and Materials Science
Soochow University, Jiangsu 215123 (China)
E-mail: hxq006@suda.edu.cn
Prof. S. Guo
Department of Materials Science & Engineering
College of Engineering, Peking University
Beijing, 100871 (China)
E-mail: guosj@pku.edu.cn
Dr. X. Zhang, Prof. G. Lu
Department of Physics and Astronomy
California State University
Northridge, CA (USA)
Dr. X. Shen, Dr. D. Su
Center for Functional Nanomaterials
Brookhaven National Laboratory
Upton, NY 11973 (USA)
[+] These authors contributed equally to this work.
Supporting information and the ORCID identification number(s) for the author(s) of this article can be found under http://dx.doi.org/10.1002/anie.201603022.

respectively. The density functional theory (DFT) calculations reveal that the improved ORR activities on the PdCuM NPs stem from the catalytically active hollow sites arising from the ligand effect and the compressive strain on the Pd surface owing to the smaller atomic size of Cu, Co, and Ni. Most importantly, they also show significantly enhanced durability for ORR with the limited activity decay under prolonged duration. Our work opens a new strategy to design a new class of non-Pt catalysts with interesting intermetallic phase tuning for further boosting the catalytic performance for fuel-cell reactions.

A simple wet-chemical method was adopted to prepare disordered PdCuM (M = non, Ni, or Co) NPs with highly monodisperse feature. Figure 1a and Figure S1 (see the Supporting Information) show representative transmission electron microscopy (TEM) and high-angle annular dark-field scanning TEM (HAADF-STEM) images of the prepared PdCu NPs. It is clearly found that the product consists of uniform NPs with spherical shape. The NPs are highly monodisperse with an average edge length of 5.1 ± 0.8 nm (inset of Figure 1a). The Pd/Cu composition is 46.20/53.80, as confirmed by scanning electron microscopy energy-dispersive X-ray spectroscopy (SEM-EDS, Figure S1), being consistent with the result of inductively coupled plasma atomic emission spectroscopy (ICP-AES). The X-ray diffraction (XRD) pattern of PdCu NPs (Figure 1b) shows that the representative diffraction peaks at 41.4, 48.2, 70.5, and 85.3° can be readily indexed to (111), (200), (220), and (311) reflections of face-centered cubic (*fcc*) PdCu (JCPDS number 48–1551). The high-resolution TEM (HRTEM) image taken from individual PdCu NP shows that it has high crystallinity, and its lattice spacing is measured to be 0.222 nm, being well consistent with the value of (111) plane of *fcc* PdCu (inset of Figure 1b).

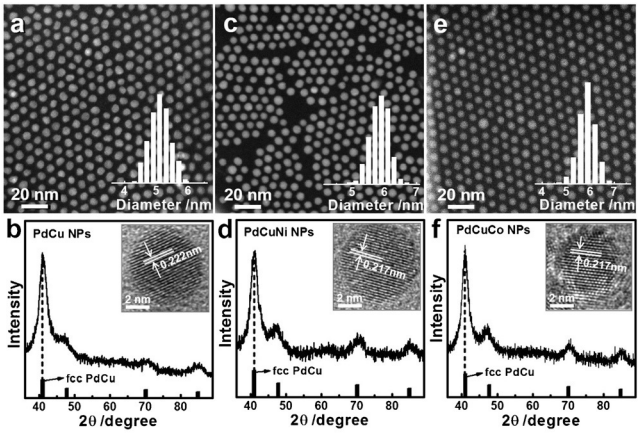

Figure 1. Representative a) HAADF-STEM image and b) XRD pattern of PdCu NPs. c) HAADF-STEM image and d) XRD pattern of PdCuNi NPs. e) HAADF-STEM image and f) XRD pattern of PdCuCo NPs.

The most important feature of the present synthetic protocols is highly general for the preparation of trimetallic PdCuNi NPs and PdCuCo NPs by simply introducing additional $Ni(acac)_2$ and $Co(acac)_2$ into the synthesis solution, respectively. Monodisperse PdCuNi NPs and PdCuCo NPs, very similar to PdCu NPs, could be readily obtained (Figure 1c–f and Figures S2,3). To further identify the formation of trimetallic PdCuNi and PdCuCo NPs, we used a number of tools to analyze the structures and characterize the chemical composition of the NPs: 1) The SEM-EDS result suggests that the molar ratio of Pd/Cu/Ni in PdCuNi NPs and Pd/Cu/Co in PdCuCo NPs is 34.62: 44.79: 20.59 and 34.88: 44.46: 20.66, respectively. 2) The lattice spacing across individual PdCuNi NP and PdCuCo NP shown in the HRTEM image is 0.217 nm (inset in Figure 1d) and 0.217 nm (inset of Figure 1f), respectively, closing to that of the (111) plane of PdCu alloy (0.218 nm), which are consistent with the X-ray diffraction (XRD) analyses (Figure 1d,f).

With highly uniform disordered PdCu NPs, PdCuNi NPs, and PdCuCo NPs at hand, we turned our attention to the creation of highly ordered intermetallic NPs by thermal annealing. To prevent NPs from aggregation under thermal annealing, and facilitate the catalytic studies, the as-prepared NPs were deposited on carbon (C, Vulcan) support before the annealing treatment (see the Experimental Section for details). To this end, these monodisperse NPs were first loaded on C support by sonicating the mixture of PdCuM NPs and C in cyclohexane, and then washed with a mixture of cyclohexane and ethanol for several times. Such treatments allowed the NPs uniformly distributed on C, with almost no shape, size, and phase change (PdCuM NPs/C, Figure 2a,d and Figure S4). With the acetic acid treatment to wash away the surfactant coating, the transition metal in the surface was also readily etch away, both of which help to activate the catalysts. As confirmed by both the SEM-EDS and ICP-AES, the compositions of PdCu, PdCuNi and PdCuCo NPs were

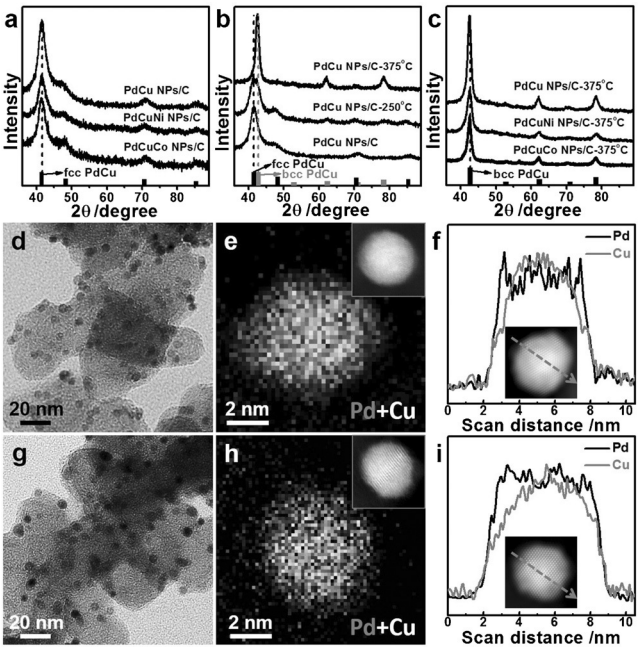

Figure 2. XRD patterns of a) PdCuM NPs/C, b) PdCu NPs/C at different heat treatment temperatures, and c) PdCuM NPs/C at 375 °C heat treatment. Representative d,g) TEM image, e,h) HAADF-STEM-EELS elemental mapping and f,i) STEM-EELS line scans of single PdCu NPs/C without and with 375 °C treatment.

tuned from Pd/Cu (46.20/53.80), Pd/Cu/Ni (34.62/44.79/20.59), and Pd/Cu/Co (34.88/44.46/20.66) into Pd/Cu (49.19/50.81), Pd/Cu/Ni (38.05/41.75/20.20), and Pd/Cu/Co (39.37/42.10/18.53), respectively. Figure 2e shows the corresponding Pd and Cu elemental mappings, where Cu is concentrated in the core region and Pd is rich in the shell. The STEM-electron energy-loss spectroscopy (EELS) line scans also confirm that Cu is concentrated in the core region, showing the formation of Pd-rich surface (Figure 2f).

Thermal annealing was then used to convert the disordered *fcc* PdCuM NPs into ordered *bcc* PdCuM NPs (M = non, Co, or Ni). It has been demonstrated that diffusion rate and ordering process of the atoms in the disordered alloy can be enhanced under the thermal annealing, which is beneficial for the formation of ordered intermetallic nanocrystals.[27,28] The structure transition of the PdCuM NPs was monitored by XRD patterns (Figure 2a–c). All initial PdCuM NPs show a typical PdCu alloy *fcc* feature. When annealed at 5% H_2 + 95% N_2 at 250°C for 1 h, the disordered PdCu NPs were converted to partially ordered PdCu NPs/C, but at 375°C for 1 h, the disordered PdCu NPs were converted to ordered PdCu NPs (body-centered cubic, *bcc*; Figure 2b). The optimized annealing condition was also applied to convert disordered PdCuNi NPs and PdCuCo NPs into ordered ones (Figure 2c). Figure S5 and Figure 2g show the typical TEM images of the PdCu NPs annealed at 250 and 375°C for 1 h, respectively. These PdCu NPs with different heating treatments can largely maintain their distributions on carbon support without any aggregation/sintering (Figure S5), and their Pd-rich surface has been largely preserved (Figure S6, Figure 2h,i).

Pd-based nanomaterials are active catalysts for various heterogeneous reactions and also show promising performance in the fuel-cell reactions, such as anodic oxidation of small organic fuels and the cathodic ORR.[29–31] The hydrogen adsorption/desorption region of the cyclic voltammetry (CV) curves in the 0.1M NaOH solution is almost negligible, as shown in Figure S7. The effect of the structure of the PdCuM NPs on ORR catalysis was first investigated, and compared with the conventional disordered PdCuM NPs and commercial Pt/C (Figure S8) and Pd/C (Figure S9). The ORR polarization curves of disordered PdCuM NPs/C and ordered PdCuM NPs/C in an O_2-saturated 0.1M NaOH solution with a sweep rate of 10 mV s^{-1} and a rotation rate of 1600 rpm are shown in Figure 3a. All the ordered PdCuM NPs/C show a positive potential shift compared with the disordered counterparts, suggesting its decreased ORR overpotential. The half-wave potentials of ordered PdCuCo NPs/C, disordered PdCuCo NPs/C, ordered PdCuNi NPs/C, disordered PdCuNi NPs/C, ordered PdCu NPs/C, and disordered PdCu NPs/C catalysts are 0.872, 0.850, 0.862, 0.841, 0.857, and 0.840 V, respectively, further indicating the enhanced activity of the ordered PdCuM NPs/C. The ORR polarization curves of all the ordered PdCuM NPs/C were further compared with the commercial Pt/C and Pd/C catalysts (Figure 3b). The mass activities at 0.9 V and 0.875 V versus reversible hydrogen electrode (RHE) for these five catalysts, determined from Figure 3b, were shown in Figure 3c,d, respectively. At 0.9 V, we can see that the ordered PdCuCo NPs/C exhibits the largest mass activity of 0.13 A mg_{Pt}^{-1} among these three ordered PdCuM NPs/C catalysts, which is 1.3 times and 3.3 times higher than those of Pt/C (0.10 A mg_{Pt}^{-1}) and the Pd/C catalysts (0.04 A mg_{Pd}^{-1}), respectively (Figure 3c and Table S1). Similar behavior was observed at 0.875 V versus RHE, where the ordered PdCuCo NPs/C also has the highest ORR activity among all the catalysts evaluated (Figure 3d).

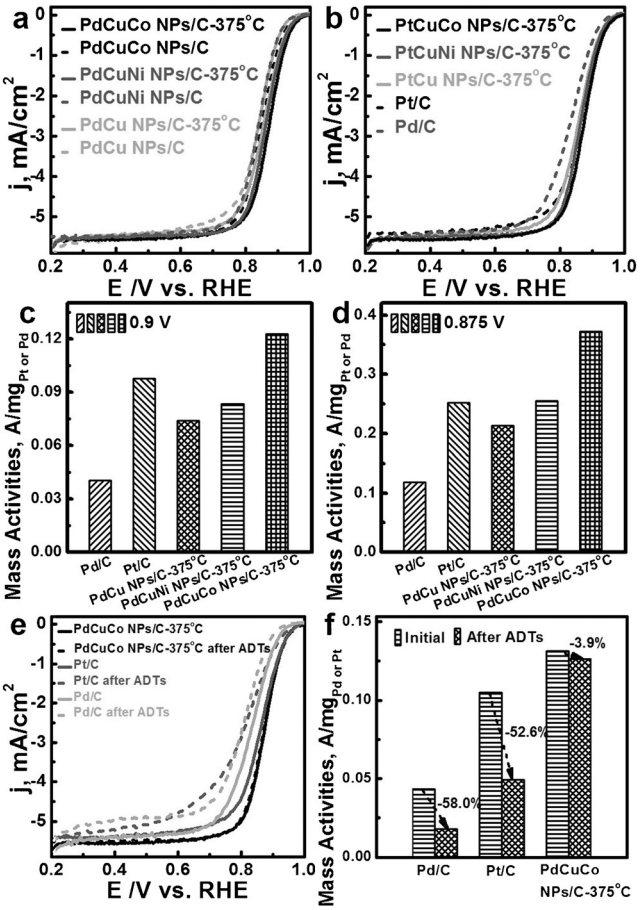

Figure 3. ORR polarization curves of a) PdCuM NPs/C and PdCuM NPs/C-375°C. b) PdCuM NPs/C-375°C, Pt/C and Pd/C recorded at room temperature in 0.1M NaOH solution. The mass activities at c) 0.9 V and d) 0.875 V versus RHE for these catalysts from Figure 3b. e) ORR polarization curves for the PdCuCo NPs/C-375°C, Pt/C and Pd/C before and after cycles of ADTs. f) Histograms of comparative mass activities at 0.90 V versus RHE for the PdCuCo NPs/C-375°C, Pt/C and Pd/C before and after cycles of ADTs.

The ordered PdCuCo NPs/C is also very stable under the ORR reaction condition. To evaluate their ORR durability, the ORR activities of the PdCuCo NPs/C were measured before and after 10000-cycle accelerated durability tests (ADTs). After 10000 sweeping cycles, there is almost no shift in ORR polarization curve for PdCuCo NPs/C (Figure 3e), while under the same condition, both commercial Pt/C and Pd/C catalysts show the obvious negative shift in ORR polarization curves (Figure 3e). As shown in Figure 3f, the ordered PdCuCo NPs/C catalyst shows only loss of 3.9% in mass activity after the 10000-cycle ADTs. Under the same condition, the Pt/C and Pd/C catalysts show the 52.6% and 58.0% loss of mass activities, respectively (Figure 3f). These

catalysts after the durability tests were also checked by TEM and SEM-EDS, showing that there is no change on the morphology and composition of the ordered PdCuCo NPs/C after 10000 cycles (Figure S10), but the serious aggregation occurred on the commercial Pt/C and Pd/C after the durability tests (Figures S8 and S9). Therefore, the ordered PdCuM NPs/C exhibit not only higher ORR activities, but also greatly enhanced catalytic durability.

To reveal the catalytic role of ordered PdCuM NPs, we conducted X-ray photoelectron spectroscopy (XPS) analysis to determine the electronic structures of the ordered PdCuM NPs and the disordered counterparts. The Pd 3d spectra of PdCu NPs show two peaks that can be assigned to the Pd $3d_{5/2}$ and Pd $3d_{3/2}$ states, and be further split into two doublets, associated with Pd^0 and Pd^{2+} chemical states. Similarly, the Cu $2p_{3/2}$ can be split into one doublet, associated with Cu^0 and Cu^{2+} chemical states (Figure S11). It is clear that the majority of the Pd and Cu atoms of these PdCu NPs are mainly in the metallic state. It is calculated that the ratio of Pd^0/Pd^{2+} in these PdCu NPs increases with the heat treatment temperature. On the contrary, their corresponding ratio of Cu^0/Cu^{2+} decreases with the heat treatment temperature, which can be due to Pd and Cu atomic ordering in PdCu NPs enhances the electronic interactions between Pd and Cu. The high ratio of Pd^0 can increase the number of free Pd sites of the ordered PdCu NPs, improving the catalytic property for more contact opportunity between reactant molecules and free Pd sites. Furthermore, compared with the binding energy of the Pd $3d_{5/2}$ peak of these PdCu NPs, we also find an increase in the order of disordered PdCu NPs and ordered PdCu NPs, indicating a strong change in the electronic structure. This change can be explained by the fact that the more uniform distribution of Cu and Pd atoms of the ordered PdCu NPs can have high coordination of Pd atoms, which is beneficial for the conversion of O_2 molecules. Similar phenomena were also observed for ordered PdCuM NPs and disordered counterparts (Figures S12 and S13), where the increase ratio of Pd^0/Pd^{2+} and the change of electronic structure were also observed because of the ordered atomic arrangement in the ordered PdCuM NPs. Briefly, the ordered structure of the PdCuM NPs can provide better opportunity for the adsorption, activation, and dissociation of small molecules, and result in an enhanced catalytic performance.

To elucidate the dependence of ORR performance on the structural order and chemical composition of PdCuM alloys, we calculated oxygen adsorption energy (E_O) at the hollow sites of the (111) surface using density functional theory (DFT). There are two or three inequivalent hollow sites on the (111) surface depending on the chemical composition, and they are labelled by red triangles (sites 1, 2, 3) in Figure 4a. E_O is widely used as a descriptor of ORR activity, and there exists an optimal value of E_O, for which the ORR activity reaches the maximum.[32,33] For convenience, this optimal E_O is shifted to 0 eV, thus ΔE_O represents the difference of a given E_O value relative to this optimal reference. It is known that the surface atoms such as Cu, Co, and Ni of the PdCuM NPs can dissolve under the electrochemical conditions and be etched away, leading to core/shell-like structures with pure Pd as the shell. Thus, the top-layer of our DFT models consists of pure

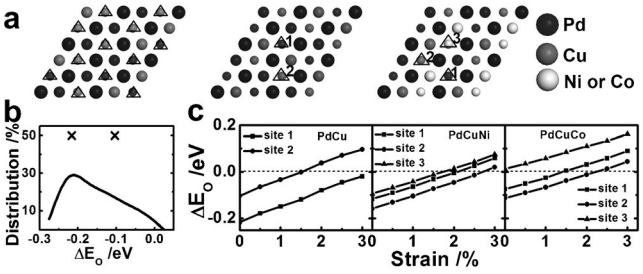

Figure 4. a) DFT models of the disordered PdCu (left), intermetallic PdCu (middle) and intermetallic PdCuM (right) alloys. The top layer consists of pure Pd. Red triangles represent the oxygen adsorption sites for the calculation of ΔE_O. b) Distribution of ΔE_O in the disordered PdCu (black curve) and intermetallic PdCu (red crosses). c) ΔE_O on the PdCu (left), PdCuNi (middle), and PdCuCo (right) (111) surface as a function of the compressive strain. The horizontal dashed line indicates the optimal ΔE_O value.

Pd as shown in Figure 4a. We first examine the effect of structural order on ORR activity by comparing E_O between the disordered and ordered PdCu alloys. The distribution of ΔE_o for the disordered PdCu peaks at −0.2 eV as shown in Figure 4b. For the intermetallic PdCu, there are two inequivalent oxygen adsorption sites with 50/50 distribution, whose ΔE_O values are −0.2 eV and −0.1 eV as indicated by the red crosses in Figure 4b. Clearly, the average ΔE_O of the ordered alloy is closer to the zero (or the maximal ORR activity) than that of the disordered alloy, suggesting that the former should exhibit higher ORR activity than the latter. The superior ORR performance of the intermetallic alloy stems from more highly active reaction sites than what are available in the disordered alloy, consistent with our XPS analysis. Next, we consider the effect of alloy composition on the ORR performance. For core/shell NPs in general both surface strain and ligand effect can influence their catalytic activities. To consider the ligand effect, we compared ΔE_O on the (111) surface of the intermetallic NPs of PdCu, PdCuNi and PdCuCo. To examine the strain effect, we calculated ΔE_O as a function of a compressive strain, ranging from 0 to 3%. As shown in Figure 4c, the hollow sites of the PdCuM alloy become more active with the addition of Ni and Co, and the ΔE_O values are consistently closer to zero as compared to PdCu. In particular, the ΔE_O values of PdCuCo are closer to zero than the two other alloys, underlying its highest ORR performance among the alloys studied. In addition, its ORR activity is found to be superior to that on the Pt NPs, consistent with the experimental observation. Furthermore, ΔE_O is shown to increase linearly as a function of the compressive strain on all the alloys, approaching zero. Thus the compressive strain can relieve the over-binding of oxygen to the surfaces, enhancing the ORR activity. Therefore, the improved ORR activities on the PdCuM NPs are attributed to: 1) the presence of the active hollow sites and 2) the presence of compressive surface strain owing to smaller atomic sizes of Cu, Co and Ni.

The ordered PdCuM NPs/C is also more active and stable for EOR than their corresponding counterparts. Figure 5a and Figure S14 show the CVs of disordered PdCuM NPs/C and ordered PdCuM NPs/C. It is obvious that the ordered

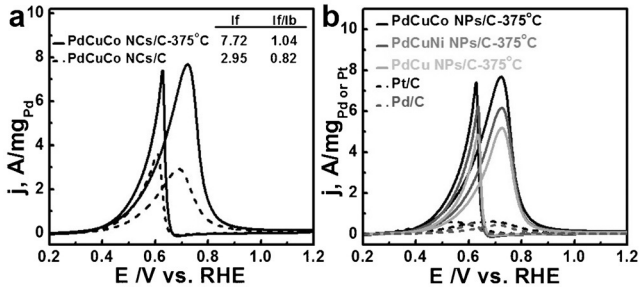

Figure 5. CVs of a) PdCuCo NPs/C and PdCuCo NPs/C-375 °C and b) PdCuM NPs/C-375 °C, Pt/C and Pd/C recorded at room temperature in the mixture of 1 M NaOH and 1 M ethanol solution with a sweep rate of 50 mV s^{-1}.

PdCuM NPs/C generally shows the higher mass activity than the disordered one. Furthermore, the ordered PdCuM NPs/C exhibits the enhanced *anti*-poisoning ability than their disordered counterparts, as the ratio of $I_{forward}$ to $I_{backward}$ of ordered PdCuM NPs for EOR is higher than that of disordered one.[34] Figure 5b compares the EOR activities of the ordered PdCuM NPs/C, commercial Pt/C, and commercial Pd/C, showing the activity increase in the order of Pd/C < Pt/C < ordered PdCu NPs/C < ordered PdCuNi NPs/C < ordered PdCuCo NPs/C (Table S1). We also found that the PdCu NPs/C-375 °C can deliver better durability than those of PdCu NPs/C-250 °C and PdCu NPs/C for EOR (Figure S15). The enhanced structure stability of the ordered PdCuM NPs/C was observed, where all the ordered PdCuM NPs/C show limited morphology/composition changes, while obvious morphology/composition changes were observed in the disordered PdCuM/C (Figures S16, S17, and S18).

To summarize, we have successfully created a new class of non-Pt electrocatalysts with interesting intermetallic phase tuning for boosting the fuel-cell reactions. These ordered PdCuM NPs are more active and stable than their corresponding disordered counterparts and also the commercial Pt/C and Pd/C catalysts towards both the ORR and EOR. Particularly, in 0.1M NaOH solution, the ordered PdCuCo NPs/C catalyst is more efficient for ORR than other ordered PdCuM NPs/C and any PdCuM NPs/C catalysts with disordered structure, suggesting such ordered PdCuM NPs can be used as a new class of high-performance electrocatalysts for future practical fuel-cells applications. This study provides a new design strategy for creating low-cost fuel-cell catalysts with both excellent electrocatalytic activity and durability.

Acknowledgements

This work was financially supported by the start-up funding from Soochow University and Peking University, and Young Thousand Talented Program, the National Natural Science Foundation of China (grant number 21571135), the Priority Academic Program Development of Jiangsu Higher Education Institutions (PAPD), the National Key Research Program (grant number SQ2016ZY02001813), theUS Army Research Office (grant number W911NF-11-1-0353), and the U.S. Department of Energy, Office of Basic Energy Sciences (grant number DE-SC0012704).

Keywords: copper · intermetallic phases · nanoparticles · oxygen-reduction reaction · palladium

How to cite: *Angew. Chem. Int. Ed.* **2016**, *55*, 9030–9035
Angew. Chem. **2016**, *128*, 9176–9181

[1] H. A. Gasteiger, N. M. Marković, *Science* **2009**, *324*, 48–49.
[2] B. C. Steele, A. Heinzel, *Nature* **2001**, *414*, 345–352.
[3] M. K. Debe, *Nature* **2012**, *486*, 43–51.
[4] W. Yu, M. D. Porosoff, J. G. Chen, *Chem. Rev.* **2012**, *112*, 5780–5817.
[5] J. Wu, H. Yang, *Acc. Chem. Res.* **2013**, *46*, 1848–1857.
[6] P. Strasser, *Science* **2015**, *349*, 379–380.
[7] J. Greeley, I. Stephens, A. Bondarenko, T. P. Johansson, H. A. Hansen, T. Jaramillo, J. Rossmeisl, I. Chorkendorff, J. K. Nørskov, *Nat. Chem.* **2009**, *1*, 552–556.
[8] N. Jung, D. Y. Chung, J. Ryu, S. J. Yoo, Y.-E. Sung, *Nano Today* **2014**, *9*, 433–456.
[9] X. Ji, K. T. Lee, R. Holden, L. Zhang, J. Zhang, G. A. Botton, M. Couillard, L. F. Nazar, *Nat. Chem.* **2010**, *2*, 286–293.
[10] Y. Li, W. Zhou, H. Wang, L. Xie, Y. Liang, F. Wei, J.-C. Idrobo, S. J. Pennycook, H. Dai, *Nat. Nanotechnol.* **2012**, *7*, 394–400.
[11] H. A. Gasteiger, S. S. Kocha, B. Sompalli, F. T. Wagner, *Appl. Catal. B* **2005**, *56*, 9–35.
[12] J. Zhang, Z. Zhao, Z. Xia, L. Dai, *Nat. Nanotechnol.* **2015**, *10*, 444–452.
[13] J. Wang, K. Wang, F.-B. Wang, X.-H. Xia, *Nat. Commun.* **2014**, *5*, 5285.
[14] G. Hu, F. Nitze, E. Gracia-Espino, J. Ma, H. R. Barzegar, T. Sharifi, X. Jia, A. Shchukarev, L. Lu, C. Ma, G. Yang, T. Wagberg, *Nat. Commun.* **2014**, *5*, 5253.
[15] Y. Lu, Y. Jiang, X. Gao, X. Wang, W. Chen, *J. Am. Chem. Soc.* **2014**, *136*, 11687–11697.
[16] A. Chen, C. Ostrom, *Chem. Rev.* **2015**, *115*, 11999–12044.
[17] Z. Fan, X. Huang, C. Tan, H. Zhang, *Chem. Sci.* **2015**, *6*, 95–111.
[18] S. Guo, X. Zhang, W. Zhu, K. He, D. Su, A. Mendoza-Garcia, S. F. Ho, G. Lu, S. Sun, *J. Am. Chem. Soc.* **2014**, *136*, 15026–15033.
[19] S. Liu, Q. Zhang, Y. Li, M. Han, L. Gu, C. Nan, J. Bao, Z. Dai, *J. Am. Chem. Soc.* **2015**, *137*, 2820–2823.
[20] C. Bianchini, P. K. Shen, *Chem. Rev.* **2009**, *109*, 4183–4206.
[21] L. Zhang, L. T. Roling, X. Wang, M. Vara, M. Chi, J. Liu, S.-I. Choi, J. Park, J. A. Herron, Z. Xie, M. Mavrikakis, Y. Xia, *Science* **2015**, *349*, 412–416.
[22] Y. Zhu, W. Zhou, Y. Chen, J. Yu, X. Xu, C. Su, M. O. Tadé, Z. Shao, *Chem. Mater.* **2015**, *27*, 3048–3054.
[23] K. C. Poon, D. C. Tan, T. D. Vo, B. Khezri, H. Su, R. D. Webster, H. Sato, *J. Am. Chem. Soc.* **2014**, *136*, 5217–5220.
[24] D. Wang, H. L. Xin, R. Hovden, H. Wang, Y. Yu, D. A. Muller, F. J. DiSalvo, H. D. Abruña, *Nat. Mater.* **2013**, *12*, 81–87.
[25] K. A. Kuttiyiel, K. Sasaki, D. Su, L. Wu, Y. Zhu, R. R. Adzic, *Nat. Commun.* **2014**, *5*, 5185.
[26] Z. Cui, L. Li, A. Manthiram, J. B. Goodenough, *J. Am. Chem. Soc.* **2015**, *137*, 7278–7281.
[27] Z. Fan, H. Zhang, *Chem. Soc. Rev.* **2016**, *45*, 63–82.
[28] W. Chen, R. Yu, L. Li, A. Wang, Q. Peng, Y. Li, *Angew. Chem. Int. Ed.* **2010**, *49*, 2917–2921; *Angew. Chem.* **2010**, *122*, 2979–2983.
[29] X. Huang, S. Tang, X. Mu, Y. Dai, G. Chen, Z. Zhou, F. Ruan, Z. Yang, N. Zheng, *Nat. Nanotechnol.* **2011**, *6*, 28–32.
[30] H. Zhang, M. Jin, Y. Xiong, B. Lim, Y. Xia, *Acc. Chem. Res.* **2012**, *45*, 1783–1794.

[31] C. Hu, H. Cheng, Y. Zhao, Y. Hu, Y. Liu, L. Dai, L. Qu, *Adv. Mater.* **2012**, *24*, 5493 – 5498.
[32] J. K. Nørskov, J. Rossmeisl, A. Logadottir, L. Lindqvist, J. R. Kitchin, T. Bligaard, H. Jonsson, *J. Phys. Chem. B* **2004**, *108*, 17886 – 17892.
[33] V. Stamenkovic, B. S. Mun, K. J. Mayrhofer, P. N. Ross, N. M. Markovic, J. Rossmeisl, J. Greeley, J. K. Nørskov, *Angew. Chem. Int. Ed.* **2006**, *45*, 2897 – 2901; *Angew. Chem.* **2006**, *118*, 2963 – 2967.
[34] A.-L. Wang, H. Xu, J.-X. Feng, L.-X. Ding, Y.-X. Tong, G.-R. Li, *J. Am. Chem. Soc.* **2013**, *135*, 10703 – 10709.

Received: March 28, 2016
Published online: June 2, 2016

